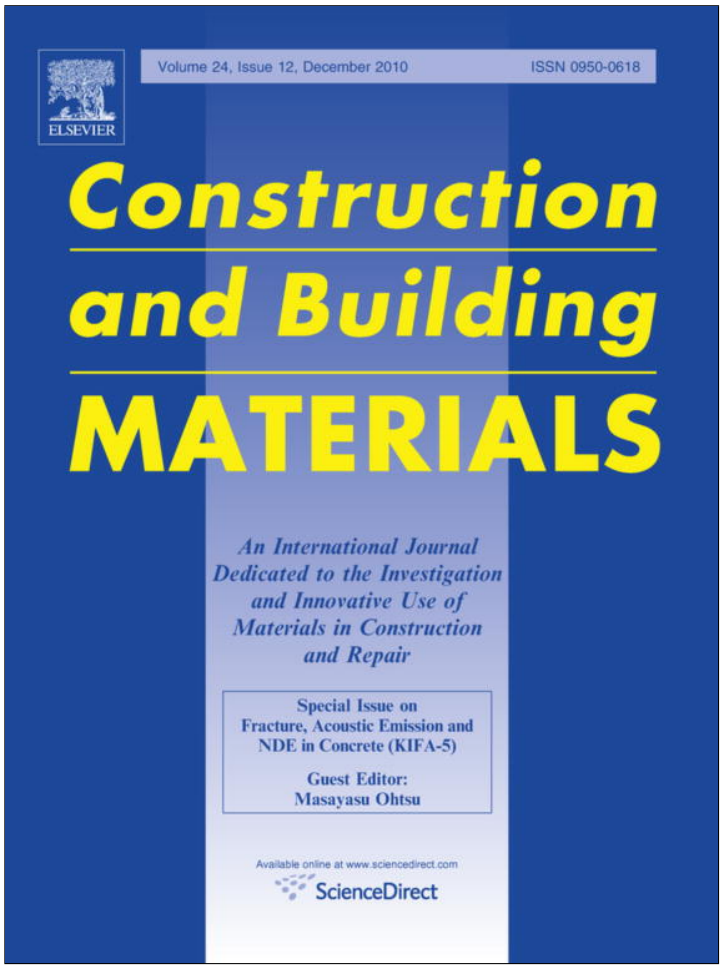

Construction and Building Materials 24 (2010) 2411–2418

Contents lists available at ScienceDirect

Construction and Building Materials

journal homepage: www.elsevier.com/locate/conbuildmat

Single-side access tomography for evaluating interior defect of concrete

H.K. Chai [a,*], D.G. Aggelis [b], S. Momoki [a], Y. Kobayashi [c], T. Shiotani [d]

[a] Research Institute of Technology, Tobishima Corporation, 5472 Kimagase, Noda, Chiba 270-0222, Japan
[b] Department of Materials Science and Engineering, University of Ioannina, Ioannina 45110, Greece
[c] College of Science and Technology, Nihon University, 8-14, Kanda-Surugadai 1-chome, Chiyoda-ku, Tokyo 101-8308, Japan
[d] Graduate School of Engineering, Kyoto University, C1-2-236, Kyoto-Daigaku-Katsura, Nishikyo-Ku, Kyoto 615-8540, Japan

ARTICLE INFO

Article history:
Received 8 March 2010
Accepted 11 March 2010
Available online 18 April 2010

Keywords:
Concrete
Tomography technique
R-waves
Phase velocity

ABSTRACT

This study investigates the suitability of surface waves in developing an innovative tomography technique for non-destructive evaluation of concrete structures. Surface waves, or specifically Rayleigh waves (R-waves), are known to exhibit strong dispersion characteristic when propagating through inhomogeneous media. Experimental program was set up to examine phase velocity change of R-waves with regard to artificial defect embedded in concrete, which could be treated as anomaly in the homogeneous medium (concrete). By adopting a multipoint source-receiver measurement only on one surface of the specimen, different sets of waveforms were excited/collected and processed to compute phase velocities of R-waves with regard to each ray path. Based on the reconstructed phase velocity tomograms, the locations of defect within the measured area could be identified or "visualized", given by regions with lower phase velocity than their neighbouring ones. It was also confirmed that the visualization was dependent on the dominant wavelengths of R-waves such that longer dominant wavelengths were able to indicate the existence of defects embedded deeper in concrete.

1. Introduction

It was estimated that in year 2025, the number of civil infrastructures, e.g. bridges and tunnels achieving more than 50 years of service age would exceed 65,000 in Japan [1]. In addition to crucial change in modern requirements for load and earthquake resistance, repair, retrofit/strengthening and maintenance of aging structures in a vast scale should request imminent attention from different authorities. In order for appropriate countermeasure to be undertaken, precise assessment of structural condition is imperative and thus the effort for development of non-destructive evaluation (NDE) methods for enhancing the effectiveness of in situ practice is underlined. Recently, extensive research in stress wave related NDE methodologies for evaluating concrete structures, e.g., ultrasonic pulse method, impact-echo method and acoustic emission method have been reported as an attempt to propose new approach for effective in situ applications [2].

Owing to rapid advancement in computer and electronic engineering technology, tomography technique is becoming a popular non-destructive method for assessing concrete structures. The tomography technique in general employs mathematic theory that reconstructs the internal condition of an object by analyzing multiple sets of projections through the object. There are several established tomography techniques, with the most commonly applied being the travel-time tomography. In this particular technique, the first arrival times for compression waves (P-waves) transmitted through an object from a source to multiple receivers located on a different side are measured and the observed data are then used for reconstructing a velocity tomogram to characterize the ray-covered region. Research and application of travel-time tomography by transmission of P-waves have been reported for different types of concrete structures. For example, Martin et al. [3] conducted tests with ultrasonic as source to investigate grouting of post-tensioned bridge beams. On the other hand, Liu and Guo [4] performed the technique with hammer impact-generated stress waves to examine the homogeneity of a concrete pier cap. Successful in situ application was also reported by Aggelis and Shiotani [5] in evaluating repair effect of a crack found on a bridge deck, and by Shiotani et al. [6,7] as well as by Miyanaga et al. [8] in confirming the repair effect of concrete piers for a water intake facility.

The travel-time tomography by transmission P-waves is straightforward in execution, but exhibits a major shortcoming as such it requires that the receivers be located on a side different from that of the source. In addition, the cost effectiveness of the method could be adversely affected when applied on structures of extensive dimensions and complicated geometries. Therefore, there is a need to enhance the efficiency and increase the versatility of the method, especially for large-scale concrete structures

* Corresponding author. Tel.: +81 4 7198 7559; fax: +81 4 7198 7586.
E-mail address: hwakian.chai@gmail.com (H.K. Chai).

0950-0618/$ - see front matter © 2010 Elsevier Ltd. All rights reserved.
doi:10.1016/j.conbuildmat.2010.03.003

that have restricted accessible face such as tunnels, bridge decks and footings.

Surface wave tomography has been used in the field of geophysics since a few decades ago as a popular means for non-invasive investigation. Surface waves are known to have the largest amplitude in waves generated by a surface impact. Also, surface waves, or in particular Rayleigh waves (R-waves) components, are dispersive in such a way that different frequencies travel at varying velocities in a stratified structure. The dispersion is often evaluated to characterize elastic properties and mass density of the propagated layers. In some previous studies for example, tomography using group velocity of surface waves was adopted to study crust structure [9,10] and to image soil structures in sedimentary basins [11] as well as waste sites [12]. The surface wave tomography is advantageous but possesses issues pertaining to the reliability of estimation, which is mainly constituted by the complexities of the structures and the indirect, computationally intensive techniques involved in the data interpretation.

Defects in concrete are often found in the form of voiding or cracking that often occupies a relatively small portion in the whole concrete volume. Considering the difference in scale, inherent nature and problems in association with soil structures and concrete, the motivation of this current study is to investigate the feasibility of using surface waves for tomography reconstruction of concrete structures for damage characterization. The aim is to develop an alternative NDE method that facilitates single-side access on concrete structures. In the experimental program, a concrete slab specimen with artificial defect introduced by thin polystyrene plates was prepared and measured to examine the change of phase velocity of R-waves caused by the defect. The observed data acquired from multi-sensor measurement, in which R-waves were generated by impacts from a steel ball hammer, were used to reconstruct two dimensional phase velocity tomograms characterizing the specimen interior. For the generation of stress waves, steel ball hammers of different ball diameters were adopted to examine the effect of R-waves of different dominant wavelengths on the evaluation result.

2. Basic concept of travel-time tomography

The travel-time tomography usually involves a methodology for reconstructing the velocity profile of a measured structure from picked travel time of stress waves. In ray theory, the travel time, t is computed from the integral of the slowness along a given ray path l

$$T = \int_l \mathrm{d}t = \int_l \frac{1}{v}\mathrm{d}l = \int_L s\mathrm{d}l \tag{1}$$

where v is the velocity, s is the slowness (reciprocal of velocity) and $\mathrm{d}l$ is the length element. By subdividing the modelling domain in M model cells of constant slowness s_i for each corresponding segment length l_i, the integral product can be summed as

$$t = \sum_{i=1}^{M} l_i s_i \tag{2}$$

Eq. (2) can be expressed in a matrix–vector form as

$$\mathbf{t} = \mathbf{L}\mathbf{s} \tag{3}$$

where $\mathbf{t}$ is the travel time vector and $\mathbf{s}$ is the vector of s_i. $\mathbf{L}$ is a matrix describing the ray path segments. Because each ray covers only a limited number of cells, the matrix is generally sparse.

Fig. 1 illustrates the general procedure involved in the tomography reconstruction. Eq. (3) is solved to simulate a velocity distribution that is able to explain the measured travel times. The ray propagation itself is a linear operator. Nevertheless, since the ray path depends on velocities, the inverse problem becomes highly non-linear and has to be solved iteratively. With a fundamental model $\mathbf{s}^0$, new models are computed successively based on the discrepancy of data and model response by solving

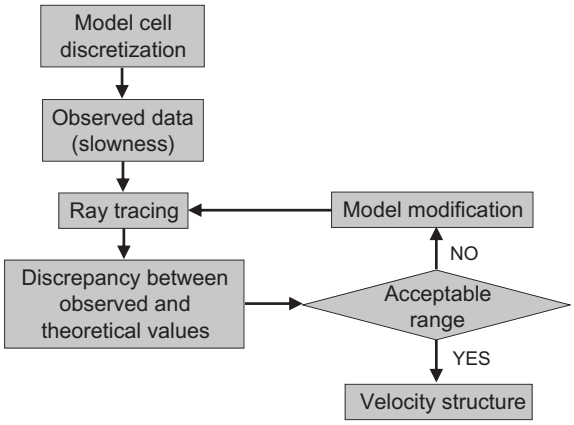

Fig. 1. Procedure for travel-time tomography reconstruction.

$$\mathbf{s}_{k+1} = \mathbf{s}^k + \Delta\mathbf{s}^k = \mathbf{s}^k + \mathbf{L}^{\dagger}(\mathbf{s}^k)(\mathbf{t} - \mathbf{L}(\mathbf{s}^k)\mathbf{s}^k) \tag{4}$$

with $\mathbf{L}$ recomputed and so on. $\mathbf{L}^{\dagger}$ is the used inverse operator.

The computation process is referred to as ray tracing. Common methodologies used for ray tracing include the algebraic reconstruction techniques (ART) and simultaneous iterative reconstruction technique (SIRT). The rays are usually restricted to the edges of the mesh and therefore a weighted shortest path problem can be solved. Travel times are always not accurately estimated in the first few iterations because not every path can be used, or there is insufficient observed data. However, with increasing refinement in the computation, the discrepancy will diminish.

3. Experiment

As shown in Fig. 2a, the specimen used in the experimental program was a 1500 × 1500 × 300 mm concrete slab. To model void in concrete, four 5 mm-thick circular polystyrene plates of 300 mm in diameter were embedded into the specimen before casting. The polystyrene plates were located at 30 mm, 60 mm, 100 mm and 140 mm from the top of one measurement surface, respectively. Therefore, from the opposite measurement surface, the depths of the plates became 160 mm, 200 mm, 240 mm and 270 mm, respectively.

The concrete mixture was prepared using ordinary Portland cement and limestone aggregates with maximum size of 20 mm. After demoulding the specimen was cured under air-dried conditions. At 28-day of age, the concrete achieved an average compression strength of 29.1 MPa and a static elastic modulus of 26.4 GPa based on tests in compliance to JIS A1108 and JSCE-G 502.

For stress wave measurement, accelerometers with a flat response up to approximately 30 kHz (Fujiceramics SAF51) were mounted on the specimen surface to form a 4 × 4 matrix arrangement as depicted in Fig. 2b. Each sensor was fixed by a screw to a small steel plate, which was bonded to the concrete using high-vacuum wax (Electron wax, Furuuchi Chemical Corp.) as the coupling agent. The distance between two adjacent sensors was fixed at 300 mm in both the vertical and horizontal directions. Similar arrangement was employed for measurement on the opposite side of the specimen. In order to measure R-wave velocity of sound concrete, nine accelerometers were attached in a straight array of 150 mm spacing, as illustrated in Fig. 3. Four locations of sound concrete were measured to compute the average.

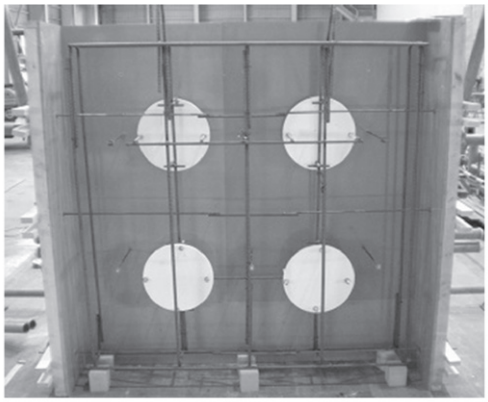

(a) Formwork of slab specimen showing embedded polysytrene plates as artificial defect

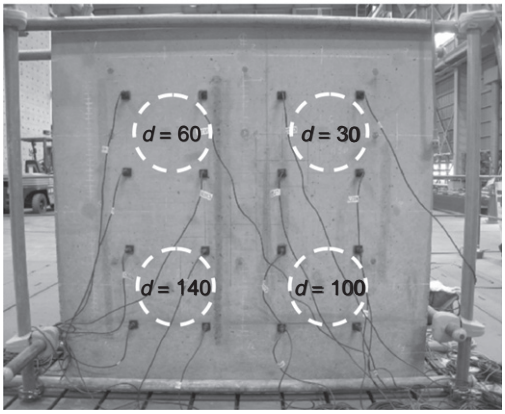

(b) Arrangment of sensor on one surface for tomography measurement
(*d*: depth of defect from the access surface; unit in mm)

Fig. 2. Specimen and arrangement of sensors.

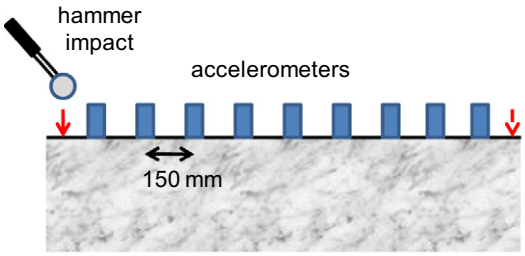

*Impacts on two sides of the sensor array

Fig. 3. Straight array measurement for R-wave velocity on sound concrete.

During the measurement, stress waves were generated by tapping the concrete surface with a steel ball hammer. With three different ball diameters of 5 mm, 8 mm and 15 mm, stress waves of different frequency characteristics were excited. A 16-channel waveform acquisition system (TEAC Instruments GX-1 System) was used to record waveform data at an interval of 5 μs for a total of 4096 samples. Each set of impact was made by continuing hitting the specimen surface with a steel ball hammer for 5 s, resulting in generating about 20 impacts in a set of waveforms recorded by each accelerometer. The impact was conducted near one accelerometer configured as the trigger, while the rest as receivers to record arriving waveforms. The acquisition was synchronized such that all channels would start recording at the same time once the trigger channel was excited. In the case for acquiring observed data for tomography reconstruction, the impact and recording process was repeated by subsequently setting the next accelerometer as the trigger, until all the 16 accelerometers have been covered. This summed up to 240 sets of waveforms for each hammer size. Fig. 4 illustrates the potential ray paths for R-waves. For measuring the R-wave velocity of sound concrete using the straight sensor array, the trigger was only configured for the outermost accelerometer in

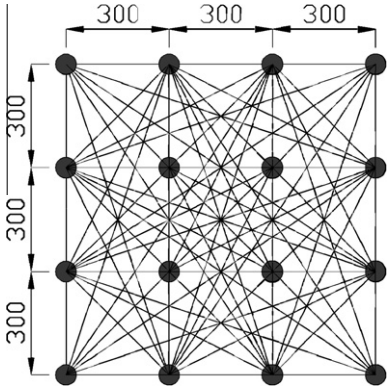

Fig. 4. Imaginary ray paths indicating propagation of R-waves (unit in mm).

the array at one end, before shifting to the opposite end. This thus generated two sets of waveform for each array and summing up to a total of eight measurements for the four locations of sound concrete. In both the measurements using straight array and matrix arrangement, each set of recorded waveform was stacked accordingly to increase sound to noise ratio before further processing.

4. Results

4.1. Waveform processing

In Fig. 5, examples of stacked time-series data acquired from the straight line measurement of sound concrete are shown. The data were pre-filtered using a tenth order Butterworth low pass filter in accordance to the theoretical response of sensor. From the waveform, the peaks of arriving R-waves could be readily recognized because they have the most energy compared to the preceding amplitudes that represent body waves [13]. Considering that wave arrival time changes linearly with travel distance in a homogeneous concrete, for waveforms recorded by sensors that were distant from the impact source, a drawn line was extended to aid identify the Rayleigh peaks that have become much less indicative because of scattering and attenuation. In Fig. 6, a typical travel time versus distance plot for the picked amplitudes is shown. The velocity of R-waves was expressed as the inverse of gradient from linear regression. The average R-wave velocities by steel ball hammers of 3 mm, 8 mm and 15 mm in diameters were marked as 2255 m/s, 2218 m/s and 2236 m/s, respectively for the sound concrete. The velocity results would serve as the reference values for sound concrete, as well as initial data for each model cell for tomography reconstruction.

Fig. 7 exemplifies a time-series data and the corresponding frequency response. The frequency response is presented as power spectral density plot computed using the fast Fourier transform (FFT) with 4096 samples. The result has several frequency peaks

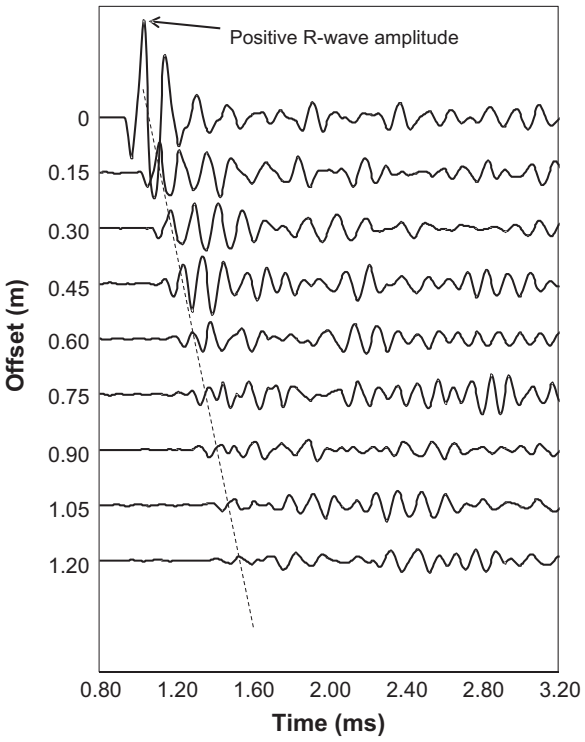

Fig. 5. Stacked time-series data obtained from measuring sound concrete with a straight array.

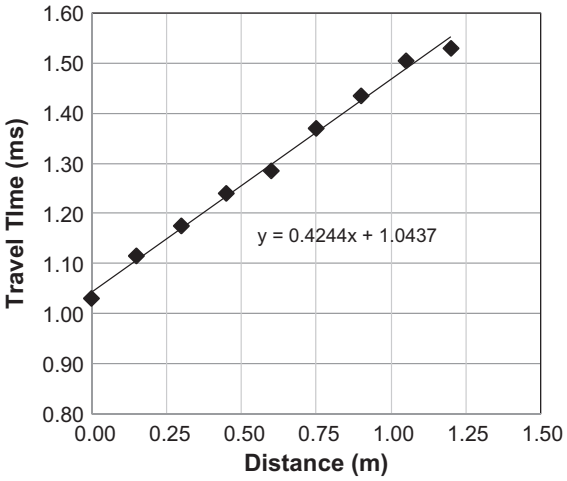

Fig. 6. Travel time versus distance plot of R-waves.

to indicate the existence of multiple frequencies that were dominating in the waveform. To enable analysis for R-waves, it was required to extract from the measured waveform information pertaining to R-waves only. This was carried out by manually processing the time-series data to retain amplitudes related to the first arriving R-waves, while "zeroing" all the preceding and subsequent amplitudes. The processing required identification of time window containing the main Rayleigh portion as anticipated based on the typical velocity of surface waves. Fig. 8 shows the processed time series and the corresponding FFT result of original waveform given in Fig. 7. Also it can be noticed that the frequency response of the processed waveform has become more clear-cut, showing a peak frequency belonging to the R-waves. Using the measured R-wave velocity and peak frequency values, the dominant wavelengths of R-waves were calculated as 110 mm, 188 mm and 240 mm for hammer diameters of 3 mm, 8 mm and 15 mm, respectively. The calculated wavelengths were later used for evaluating the accessible depth of defect by R-waves with reference to the tomography reconstruction results.

4.2. Tomography reconstruction using phase velocity

Phase velocity of R-waves was computed using the following equation:

$$V_{ph} = \lambda f = \left(\frac{2\pi\Delta x}{\Delta\phi}\right) f \tag{5}$$

where V_{ph} is the phase velocity, λ is the wavelength, f is the frequency, Δx is the distance between trigger and receiver, and $\Delta\phi$ is the phase difference (in radian) between the waveforms of trigger and receiver at f frequency [14]. Fig. 9 gives typical V_{ph} versus f curves for both cases of R-waves propagating on the sound concrete as well as the portion embedded with defect, computed using data of hammer with ball diameter of 15 mm. It is also to be noted that the calculated dominant wavelength was greater in magnitude than the defect depth, which was located 30 mm from the measurement surface. Within the selected frequency range, it can be noticed that V_{ph} was in the range of 2250–2500 m/s for the case of sound concrete. The results tallied with the ones acquired from measuring the sound concrete using a straight array. On the other hand, it was also indicated that for propagation paths containing the defect, R-wave velocity in general has decreased to less than approximately 1900 m/s. The decrease inferred that the energy of R-waves has penetrated deep enough to be distorted or dispersed by the defect to result in a different behaviour of propagation. It was also

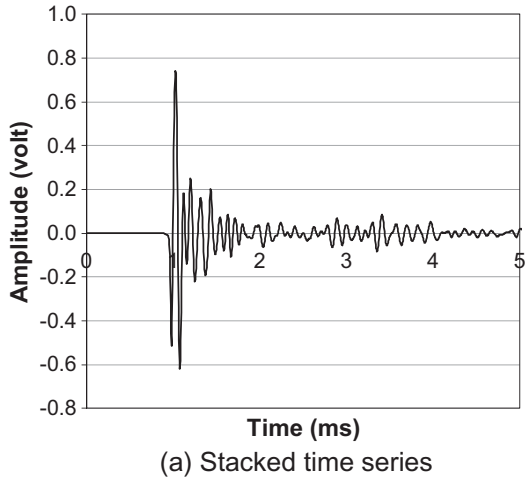

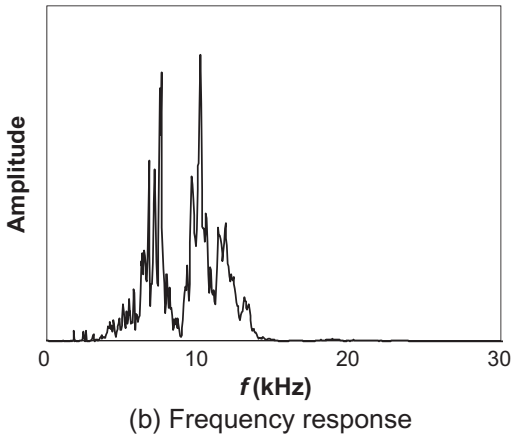

Fig. 7. Typical waveform recorded during measurement and the corresponding frequency response.

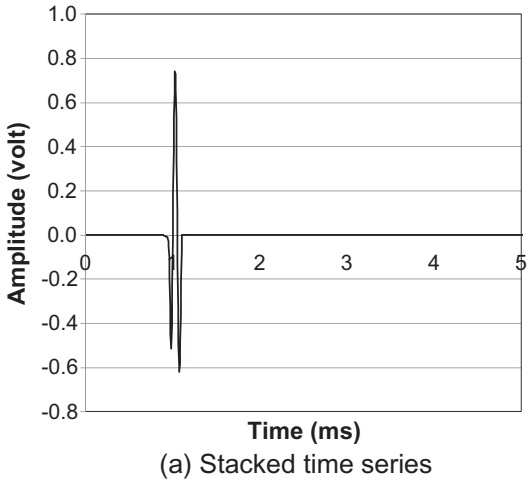

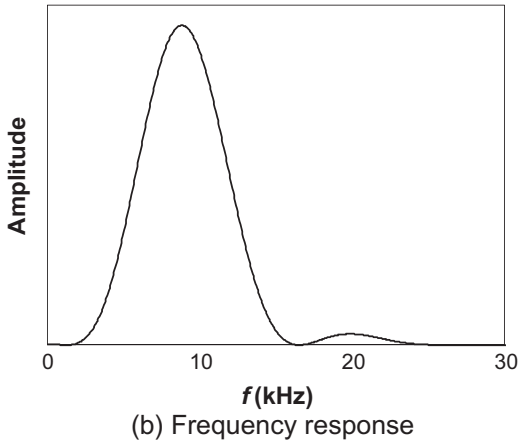

Fig. 8. Processed waveform and the corresponding frequency response for R-waves.

noted that for most of the other measured data with defect depth greater than the dominant wavelength of R-waves, similar trend as shown in Fig. 8 prevailed. Taking into account the size of defects, specifically their small thickness, the phase velocity decrease of approximately 500 m/s can be regarded as sensitive in manifesting the effect of an anomaly has on the behaviour of R-waves.

For tomography reconstruction, a 6 × 6 square mesh of 150 mm was adopted to model the measured area. The V_{ph} values at peak frequencies corresponding to the respective hammer diameters were used as the observed data at the measured locations. The computation was carried out using SIRT procedure-based algorithm for 20 iterations to achieve satisfactory convergence. Figs. 10 and 11 present the results of tomography reconstruction, expressed in the form of V_{ph} distributions for measurements on the surfaces with relatively small defect depths (30–140 mm) and large defect depths (160–270 mm), respectively. Based on Fig. 10, it can be found that the 3 mm-ball hammer, which generated R-waves with a calculated dominant wavelength of 110 mm, was less effective in visualizing defect with depth of 100 mm, and did not exhibit any sensitivity to the existence of the defect that was located 140 mm from the measurement surface. Visualization for the defect of 100 mm deep was significantly enhanced by using the 8 mm ball hammer that generated a calculated dominant wavelength of 188 mm. However, visualization for the 140 mm-deep defect was only achieved with the use of 15 mm ball hammer that yielded a calculated dominant wavelength of 240 mm. It is to be noted also that the circular shape of the defects was not accurately represented by the low V_{ph} region. In most cases the centre

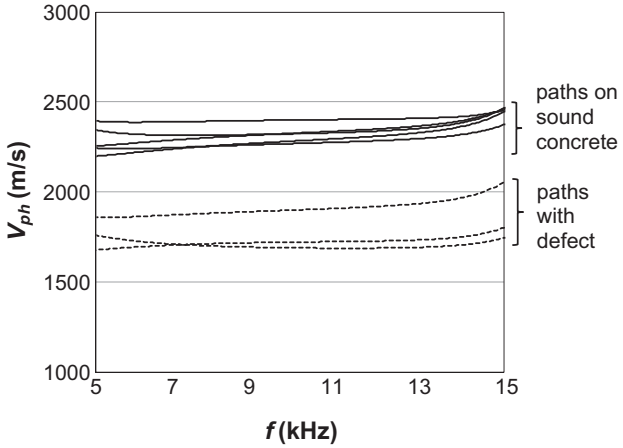

Fig. 9. V_{ph} versus f plot for selected data.

of defect was marked by the lowest V_{ph} velocity ranged in the gradation scale, and the change of V_{ph} from the centre to the edge of defects developed in unsymmetrical ways.

On the other hand, by studying the tomography results given in Fig. 11 for the opposite measurement surface, it was understood that none of the defects could be visualized by the 3 mm and 8 mm ball hammers. For the 15 mm ball hammers, visualization was suggestive, although with lesser contrast in the change of

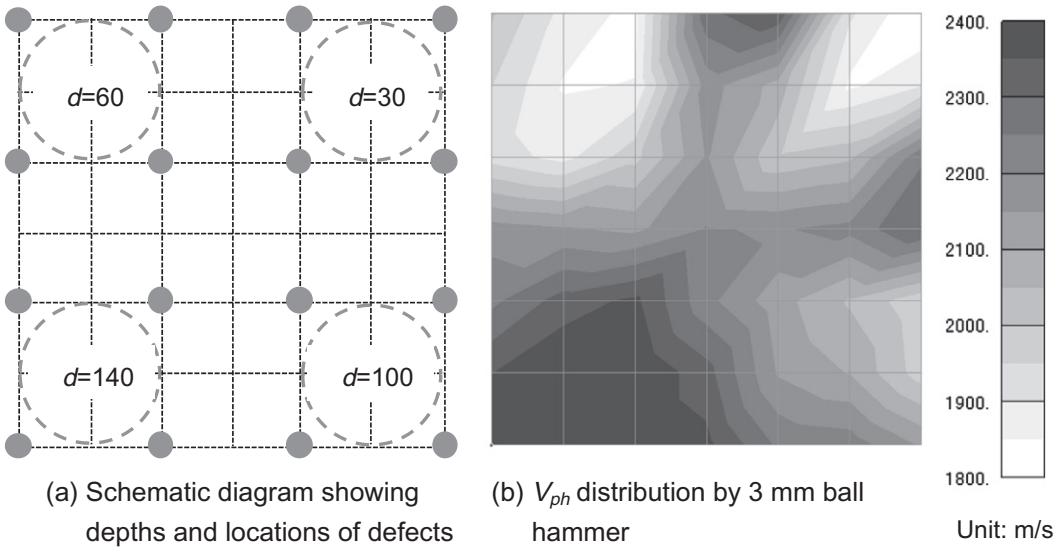

(a) Schematic diagram showing depths and locations of defects (*d*: depth; unit in mm)

(b) V_{ph} distribution by 3 mm ball hammer

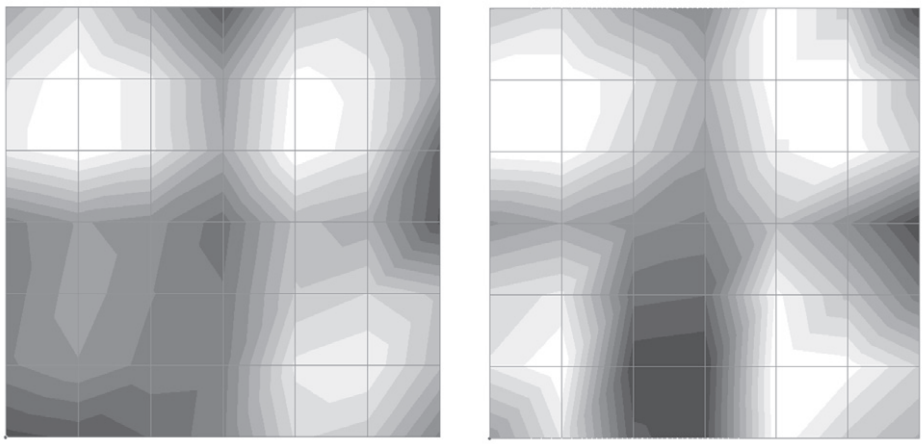

(c) V_{ph} distribution by 8 mm ball hammer

(d) V_{ph} distribution by 15 mm ball hammer

Fig. 10. Tomography reconstruction results for measurement on surface with relatively small defect depths.

V_{ph}, for the defects with relatively small depths of 160 mm and 200 mm, but far less indicative for the other two defects which were deeper. This implied that although R-waves were generated from the same impact sources, their energy penetration from this measurement surface was not affected by defects that were deeper than approximately one wavelength of R-waves, which depths have become greater as measured from this surface of access. Furthermore, from the results it was demonstrated that the accuracy of assessment by tomography were dependable upon the dominant wavelength of the generated R-waves.

5. Discussion

As with most of the actual concrete structures, the specimen adopted in this study has finite dimensions. Its free boundaries tended to instigate multiple phenomena related to stress wave propagation, such as reflections, mode conversions and convergence of body waves from different directions. Since the reflected body waves travelled with a velocity higher than a direct R-waves, for long propagations the R-waves of interest could have been masked because their energy was "contaminated" by the reflected body waves. Although the waveform processing method employed in this current study can eliminate the influence of preceding and subsequent waves, complete removal of undesired energy or frequency components from the pure R-waves was not possible. Moreover, it is to be noted that the method has called for manual processing of waveforms. To minimize uncertainties, waveforms which were not recognizable for large amplitudes related to first arrival of R-waves, specifically those recorded for long-distance propagations were discarded from further analysis.

Dispersion of R-waves is pronounced in thick layered structures with the layers extend almost uniformly over an area of virtually unlimited planar dimensions. This condition makes R-waves very suitable for geophysical prospecting purposes, for example to evaluate the profile of geotechnical materials. In this current study, however, the inhomogeneity was modelled as a type of defect resembling cracking or voiding inside concrete, which often have ineligible relative dimensions. With regard to such a defective condition, in which the defect thickness was 5 mm while the specimen thickness was 300 mm, although distortion could be confirmed, as

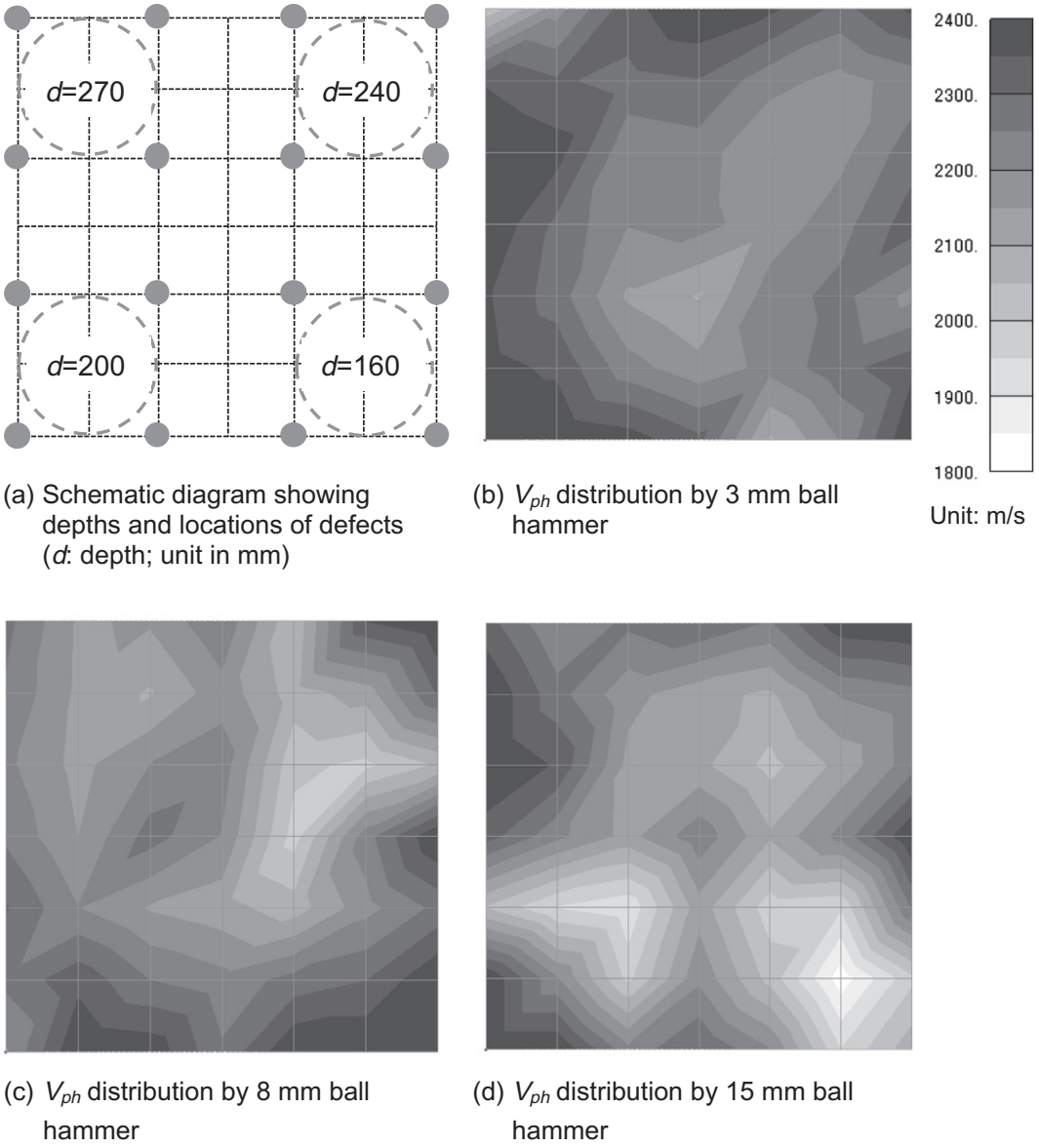

(a) Schematic diagram showing depths and locations of defects (*d*: depth; unit in mm)

(b) V_{ph} distribution by 3 mm ball hammer

(c) V_{ph} distribution by 8 mm ball hammer

(d) V_{ph} distribution by 15 mm ball hammer

Fig. 11. Tomography reconstruction results for measurement on surface with relatively large defect depths.

demonstrated by the change of phase velocity, dispersion of R-waves was less suggestive for the selected frequency range. This was because the resulted dispersion curves did not give different phase velocity for particular frequency components that correspond to the thickness location of defect. Conversely, the decrease was almost uniform throughout the selected frequency range.

R-waves are known to be propagating through a zone that is approximately one wavelength deep [15]. Based on literature study, however, it is found that the penetration depth varied in accordance to material as well as structural form. For example, Wardany et al. [16] reported satisfactory estimation for elastic properties of layered concrete slabs by assuming the effective R-wave penetration depth to be equivalent to half a wavelength. On the other hand, a study using concrete beams concluded that at vertical distances greater than half the beam depth, R-waves did not formed because of the fundamental modes diverged at longer wavelengths and energy was consumed in flexural mode [17]. In another study on determining the near-surface profile of soil structures by Kacouglu and Long [11], it is stated that R-wave velocity was determined primarily by the shear wave (S-wave) velocity of material in a depth range of 1/4 wavelength. In this current study, the visualization for defect by phase velocity change is considered to be effective for less than one wavelength of R-waves based on the experimental findings. Although the feasibility of R-wave phase velocity for developing a tomography technique that accesses only one measurement surface was demonstrated, further work would be essential to investigate the dispersive behaviour of R-waves (frequency dependence of velocity) in such a defective condition. Furthermore, it would be desired to clarify the quantitative relation between dominant wavelength of R-waves and the depth of defect that causes distortion, so that the vertical location of defect can be estimated in a more accurate way. In any case however, it is worth mentioning that even if a defect is not visualized at its actual dimensions using the proposed methods, successful detection for the fingerprint of the defect would help provide useful information for minimizing the labour and increasing the effectiveness of other pinpoint NDE techniques, such as the impact-echo method [18], to characterize in detail the defective area.

6. Conclusion

The feasibility of R-waves for developing a single-side access tomography technique of concrete was investigated experimentally. By generating stress waves with man-made hammer impacts, measurements were carried out using a multi sensor arrangement on a concrete slab specimen induced with artificial defects. To minimize the influence of reflected body waves from the free boundaries of the specimen, the acquired waveforms were pre-processed manually to extract the first arriving R-waves, and resulted in yielding single-peak frequency responses that was related only to the R-waves of interest. Results showed that phase velocities of R-waves were very sensitive to the embedded defect. The decrease of phase velocity was found to be uniform throughout the selected frequency range of investigation without exhibiting characteristic peaks. Nevertheless, distortion of R-wave energy by the defect was pronounced by the translation of the whole dispersion curve to lower values, especially for the longer wavelength excitation. Tomography reconstructions results indicated the suitability of the measurement method and data analysis procedure for visualizing subsurface defects. It was demonstrated that by increasing the dominant wavelength of R-waves, wave penetration could be improved and deeper defect could be detected. Studies on the quantitative relation between dominant wavelength and depth of defect, in addition to clarifying the dispersion characteristic of R-waves, are imperative in future in order to realize accurate assessment of concrete structures using the proposed tomography technique. Numerical simulations are expected to greatly enhance our knowledge concerning the interaction between dominant wavelength and depth of defect that can be identified.

Acknowledgement

This work is partially supported under Grant-in-Aid for Young Scientists (Grant no: 20860100) by Japan Society of the Promotion of Science.

References

[1] White paper on land, infrastructure, transport and tourism: Ministry of Land, Infrastructure, Transport and Tourism, Japan; 2006. <http://www.mlit.go.jp/hakusyo/mlit/h18/hakusho/h19/index.html>.
[2] Technical report and symposium proceedings of committee on non-destructive testing of concrete by elastic wave methods: Japan Society of Civil Engineers; 2004 [in Japanese].
[3] Martin J, Broughton KJ, Giannopolous A, Hardy MSA, Forde MC. Ultrasonic tomography of grouted duct post-tensioned reinforced concrete bridge beams. NDT E Int 2001;34:107–13.
[4] Liu L, Guo T. Seismic non-destructive testing on a reinforced concrete bridge column using tomographic imaging techniques. J Geophys Eng 2005;2:23–31.
[5] Aggelis DG, Shiotani T. Repair evaluation of concrete cracks using surface and through-transmission wave measurements. Cem Concr Compos 2007;29:700–11.
[6] Shiotani T, Momoki S, Chai HK, Aggelis DG. Elastic wave validation of large concrete structures repaired by means of cement grouting. Constr Build Mater 2009;23(7):2647–52.
[7] Shiotani T, Aggelis DG, Momoki S. Damage evaluation of concrete structures by seismic tomography. Tobishima Tech Rep 2007;56:111–6 [in Japanese].
[8] Miyanaga T, Kuroki H, Momoki S. Evaluating repair effect of concrete structures by three-dimensional elastic wave tomography. Elec Pow Civil Eng 2010;345:16–20 [in Japanese].
[9] Tarr AC. Rayleigh-wave dispersion in the North Atlantic Ocean, Caribbean Sea, and Gulf of Mexico. J Geophys Res 1969;74:1591–607.
[10] He Z, Ding Z, Ye T, Sun W, Zhang N. Surface wave tomography of the crust and upper mantle of Chinese mainland and its neighbouring region. Acta Seism Sinica 2001;14(6):634–41.
[11] Kacaoglu AH, Long LT. Tomographic inversion of RG wave group velocities for regional near-surface velocity structure. J Geophys Res 1993;98(B4):6579–87.
[12] Long LT, Kacaoglu A. Surface-wave group-velocity tomography for shallow structures. J Environ Eng Geophys 2001;6(2):71–81.
[13] Qixian L, Bungey JH. Using compression wave ultrasonic transducers to measure the velocity of surface waves and hence determine dynamic modulus of elasticity for concrete. Constr Build Mater 1996;10(4):237–42.
[14] Sachse W, Pao YH. On the determination of phase and group velocities of dispersive waves in solids. J Appl Phys 1978;49:4320–7.
[15] Graff KF. Wave motion in elastic solids. New York: Dover; 1991.
[16] Wardany RA, Ballivy G, Gallias J, Saleh K, Rhazi J. Assessment of concrete slab quality and layering by guided and surface wave testing. ACI Mater J 2007;104(3):268–75.
[17] Zerwer A, Polak MA, Santamarina JC. Detection of surface breaking cracks in concrete members using Rayleigh waves. J Environ Eng Geophys 2005;10(3):295–306.
[18] Sansalone MJ, Streett WB. Impact-echo: nondestructive evaluation of concrete and masonry. New York: Bullbrier Press; 1997.